Impact of Atmospheric Blocking on South America in Austral Summer

REGINA R. RODRIGUES

Department of Geosciences, Federal University of Santa Catarina, Florianópolis, Brazil, and Atmospheric, Oceanic and Planetary Physics, Department of Physics, University of Oxford, Oxford, United Kingdom

TIM WOOLLINGS

Atmospheric, Oceanic and Planetary Physics, Department of Physics, University of Oxford, Oxford, United Kingdom

(Manuscript received 6 July 2016, in final form 4 October 2016)

ABSTRACT

This study investigates atmospheric blocking over eastern South America in austral summer for the period of 1979–2014. The results show that blocking over this area is a consequence of propagating Rossby waves that grow to large amplitudes and eventually break anticyclonically over subtropical South America (SSA). The SSA blocking can prevent the establishment of the South Atlantic convergence zone (SACZ). As such, years with more blocking days coincide with years with fewer SACZ days and reduced precipitation. Convection mainly over the Indian Ocean associated with Madden–Julian oscillation (MJO) phases 1 and 2 can trigger the wave train that leads to SSA blocking whereas convection over the western/central Pacific associated with phases 6 and 7 is more likely to lead to SACZ events. It is found that the MJO is a key source of long-term variability in SSA blocking frequency. The wave packets associated with SSA blocking and SACZ episodes differ not only in their origin but also in their phase and refraction pattern. The tropopause-based methodology used here is proven to reliably identify events that lead to extremes of surface temperature and precipitation over SSA. Up to 80% of warm surface air temperature extremes occur simultaneously with SSA blocking events. The frequency of SSA blocking days is highly anticorrelated with the rainfall over southeast Brazil. The worst droughts in this area, during the summers of 1984, 2001, and 2014, are linked to record high numbers of SSA blocking days. The persistence of these events is also important in generating the extreme impacts.

1. Introduction

Atmospheric blocking represents an important feature for regional climate and weather patterns and plays an important role in extreme events of temperature and precipitation (e.g., Buehler et al. 2011; Sillmann et al. 2011). Blocking is often associated with heat waves and droughts in the summer and conversely with cold spells in the winter. For this reason, much effort has been made over the years to improve our understanding of the physical mechanisms related to the intensity and frequency of atmospheric blocking, particularly for the Northern Hemisphere. Blocking is often related to the breaking of Rossby waves (e.g., Pelly and Hoskins 2003), which occurs on a larger scale than the transient, filamentary, equatorward, LC1-type breaking of Thorncroft et al. (1993).

In the Southern Hemisphere, several studies show that traditional midlatitude blocking, resulting from persistent large-scale Rossby wave breaking associated with the split of the jet, occurs mainly in the western Pacific sector (Trenberth and Mo 1985; Wright 1994; Tibaldi et al. 1994; Berrisford et al. 2007; O'Kane et al. 2013; and references therein). Blocking in this area exerts great influence on Australian weather and climate and for this reason it has been comprehensively described in the literature (Pook et al. 2013; Parker et al. 2014; Reeder et al. 2015). The wave breaking produces low-level anticyclonic circulation that is often associated with heat waves and suppression of rainfall over southern Australia, which in turn is responsible for the most destructive wildfires (Parker et al. 2014; Reeder et al. 2015). Moreover, cutoff lows occur simultaneously on the equatorward side of the high, leading to excess precipitation in northeastern Australia (Pook et al. 2013; Reeder et al. 2015).

Persistent anomalous anticyclonic circulation can occur over subtropical South America during the wet

Corresponding author e-mail: Regina R. Rodrigues, regina.rodrigues@ufsc.br

DOI: 10.1175/JCLI-D-16-0493.1

season in austral summer, causing deficient rainfall (Coelho et al. 2016a,b). However, most studies of Southern Hemisphere blocking do not identify subtropical South America as a region where blocking occurs. This might be related to the methodology commonly used based on the reversal of the meridional geopotential height gradient (Damião Mendes and Cavalcanti 2014; Oliveira et al. 2014). In contrast, Berrisford et al. (2007) used a potential vorticity approach and did identify anticyclonic wave-breaking episodes in the South American–western South Atlantic sector during summer. They noticed that the wave-breaking structure in these cases was not equivalent barotropic and did not block the westerly flow, partially because they are located on the equatorward side of the jet. As such, these subtropical wave-breaking episodes were not considered by the authors to be examples of blocking. Moreover, they did not investigate the impacts of these wave-breaking episodes on surface properties such as precipitation and air temperature. There is naturally some disagreement between studies on whether such low-latitude events should be classed as blocking (Davini et al. 2012).

The South Atlantic convergence zone (SACZ) is the main source of rainfall for subtropical South America (Vera et al. 2006; Marengo et al. 2012) and is characterized by a band of strong precipitation oriented northwest–southeast, from the Amazon, over southeast Brazil toward the western South Atlantic (Liebmann et al. 1999; Carvalho et al. 2004). The area of southeast Brazil is heavily populated, home to more than 80 million people, and responsible for 60% of the Brazilian gross domestic product. Failure in the development of the SACZ in the summer can lead to water, food, and power shortages. For instance, the summer of 2013/14 was unprecedentedly dry, resulting in the worst water shortage in São Paulo's history (Coelho et al. 2016a,b). This event was linked to a persistent anomalous anticyclonic circulation over southeast South America that prevented the establishment of the SACZ.

Earlier studies have shown that the SACZ varies strongly on intraseasonal time scales and for this reason the Madden–Julian oscillation (MJO; Madden and Julian 1994) can modulate the SACZ (Nogués-Paegle and Mo 1997; Carvalho et al. 2002, 2004; Liebmann et al. 2004; Gonzalez and Vera 2014). The MJO represents a coupled pattern between atmospheric circulation and tropical deep convection that propagates eastward around the global tropics with a periodicity of approximately 30–60 days [for a comprehensive review, see Zhang (2005)]. The MJO influences the phase of the midlatitude synoptic disturbances that affect the SACZ (Liebmann et al. 2004). When convection is stronger near the date line and suppressed over Indonesia, the SACZ tends to be enhanced (Nogués-Paegle and Mo 1997; Carvalho et al. 2004). It is not clear if the MJO can also be related to persistent anomalous anticyclonic circulation, which then prevents the establishment of the SACZ, such as the event of the summer of 2013/14.

The goal of this study is to examine the subtropical South America wave-breaking events of Berrisford et al. (2007) in more detail, by assessing their links to tropospheric circulation and surface impacts. We will show that these events do have much in common with summertime midlatitude blocking, in particular in their association with high surface temperatures and deficient rainfall. The anomalous summer of 2013/14 is a striking example of the societal impact of these events. We also aim to improve our understanding of the mechanisms that lead to wave breaking over this region, in order to potentially increase our capability of forecasting such events.

2. Data and methodology

The data used in this study to compute the wave-breaking index and the composites are obtained from the European Centre for Medium-Range Weather Forecasts (ECMWF) ERA-Interim reanalysis for the period of 1979–2014 (Dee et al. 2011). Daily values are obtained by averaging the 6-hourly data of potential temperature, geopotential height, zonal and meridional components of the wind, mean sea level pressure, and 2-m temperature. We also use the $1° \times 1°$ gridded daily rainfall data provided by the Global Precipitation Climatology Project (GPCP) for the period 1997–2014 (Huffman et al. 2001), the interpolated outgoing longwave radiation (OLR) data by Liebmann and Smith (1996) as a proxy for tropical convection for the period of 1979–2014, the OLR MJO index provided by Kiladis et al. (2014) for the same period, and the $¼° \times ¼°$ gridded daily sea surface temperature (SST) data from Optimum Interpolation SST (OISST) for the period 1982–2014 (Reynolds et al. 2007).

Here, we use the methodology adapted by Berrisford et al. (2007) from Pelly and Hoskins (2003) to compute an instantaneous 2D wave-breaking index. It is based on potential vorticity (PV)–potential temperature diagnostics. The premise for the formation of a block is that a substantial mass of low PV subtropical air on a potential temperature surface is advected poleward and high PV midlatitude air is advected equatorward. In the absence of diabatic processes, potential temperature is conserved on a PV surface and we can then define the wave breaking as a reversal of the gradient of potential temperature on the dynamical tropopause, taken as the surface where PV is equal to -2 PV units

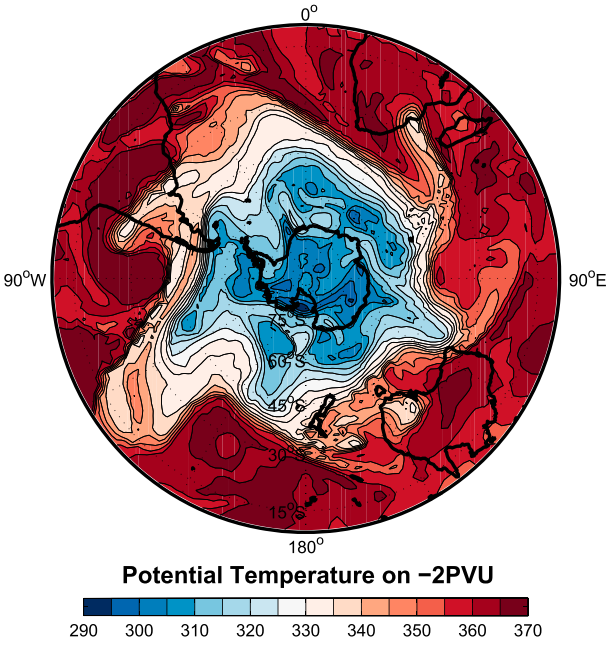

FIG. 1. Potential temperature (K) on the tropopause (−2 PVU surface) for the onset day (15 Jan 2014) of the longest blocking event over the South America-South Atlantic sector.

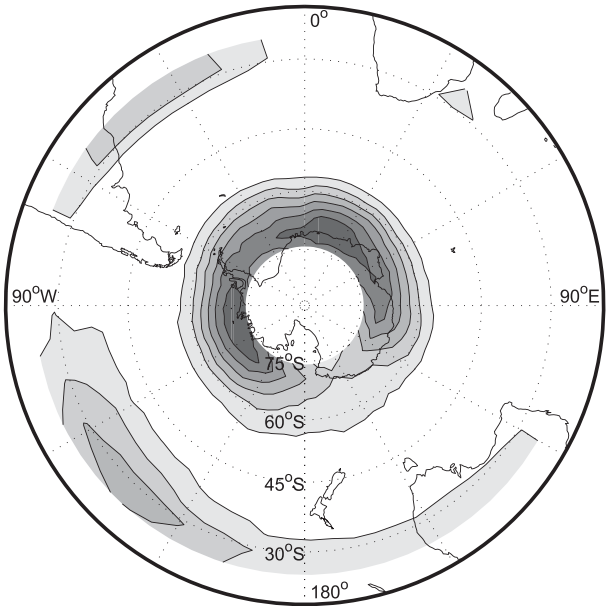

FIG. 2. Mean wave-breaking episode frequency for DJFM during the period 1979–2014. The contour interval is 5% and the zero contour is omitted. Shading starts at 5% and gets gradually darker with increasing contour level.

(PVU; $1\,\mathrm{PVU} = 10^{-6}\,\mathrm{K\,m^2\,s^{-1}\,kg^{-1}}$) in the Southern Hemisphere. As an example, Fig. 1 shows the potential temperature at −2 PVU for a day during a wave-breaking episode over the South American–South Atlantic sector (15°–45°S, 30°–70°W). Pelly and Hoskins (2003) pointed out that the Lagrangian behavior is more evident in the potential temperature field on the tropopause than in the upper-troposphere height field, hence our choice of methodology.

We test for wave breaking at all locations between 25° and 75°S, on a grid with spacing of 4° latitude and 5° longitude. Boxes with dimensions of 15° latitude by 5° longitude are defined to the south and north of each central location and the potential temperature is averaged over these areas [similar to Fig. 2 from Pelly and Hoskins (2003)]. The northern box average is then subtracted from the southern box average to give a large-scale measure of the meridional potential temperature gradient. Instantaneous wave breaking occurs when the wave-breaking index is positive (i.e., when the potential temperature in the southern box is higher than that in the northern box). However, to be considered a large-scale wave breaking, the index has to be positive for a minimum of 15° of longitude, approximately 1100 km in the midlatitudes. A wave-breaking event is said to occur at a specific longitude when large-scale wave breaking is detected within 10° of longitude of it. This index is part of a large family of reversal blocking indices that generally identify similar features [see Barriopedro et al. (2010) for a review].

Instantaneous wave-breaking events as described so far do not take into account the longevity of the reversal. Therefore, a wave-breaking episode is said to occur at a particular location when a wave-breaking event remains there for four consecutive days. Finally, the wave-breaking episode frequency is defined as the percentage of days when a wave-breaking episode occurs within a specific season.

3. Characterization of wave breaking over subtropical South America

Figure 2 shows the mean wave-breaking frequency for austral summer during 1979–2014. As expected, the spatial distribution of wave-breaking frequency is very similar to that obtained by Berrisford et al. (2007, their Fig. 8); that is, wave breaking is more frequent in high latitudes with values above 20% and peak values greater than 30% over the coast of Antarctica. In the midlatitudes, wave breaking is very weak but there are two regions of higher-frequency wave breaking in the lower latitudes, namely in the Australian–east Pacific and South American–mid-Atlantic sectors (up to 10%–15% and 15%–20%, respectively). The preference for wave breaking at these two sectors in the Southern Hemisphere is due to the slowdown of the jet there. Wave

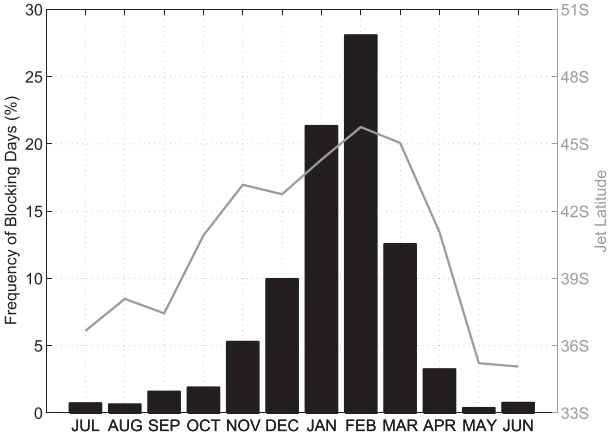

FIG. 3. Histogram of frequency of SSA blocking days per month for the period of 1979–2014 (left axis). Solid line represents the mean latitude of the jet in the South Atlantic sector averaged over 0°–60°W (right axis).

breaking tends to occur where the jet weakens, as we shall see later on. This behavior is also seen in the Northern Hemisphere (e.g., Gabriel and Peters 2008; Masato et al. 2009). In contrast, wave breaking is absent where the jet is strong and thus serves as a good waveguide, such as over the east Atlantic–Indian Ocean sector.

Since the objective of this study is to investigate the impact of wave breaking on South America in austral summer, from now on we will focus on the wave breaking over the subtropical South American–mid-Atlantic sector. We take all grid points in this sector where the mean wave-breaking frequency is above 5% (Fig. 2) and use this area to define subtropical South America (SSA) blocking. Here, we define blocking as the large-scale wave-breaking episodes captured by our index. The annual distribution of SSA blocking frequency shows that austral summer [December–February (DJF)] is the period with most SSA blocking days (Fig. 3). However, March also presents a high number of SSA blocking frequency surpassing December. For this reason, we will include March in our analyses for austral summer [December–March (DJFM)]. For the 36-yr period of 1979–2014, we found a summer blocking frequency of 17.7% over SSA (772 out of a possible 4356 DJFM days). For comparison, this magnitude is very similar to that encountered by Barnes et al. (2012) for blocking over the Euro-Atlantic sector in boreal summer. Figure 3 also shows the seasonal cycle of the eddy-driven jet latitude in the South Atlantic, following the methodology of Woollings et al. (2014). This shows a poleward migration of the jet from October to February, with SSA blocking occurring on the equatorward side of the jet during the months when it is positioned farthest poleward. As a consequence, there is a larger region of weak westerlies and anticyclonic shear on the equatorward side of the jet so that large-scale wave breaking can occur there. This is similar to the equatorward flank of the Northern Hemisphere jet streams (e.g., Gabriel and Peters 2008).

We have also computed the duration of blocking events (Fig. 4) since, as we shall see, persistence of blocking days leads to stronger extremes of temperature and precipitation. We first define the onset day as the first day considered as part of a blocking episode, after 4 consecutive days without blocking. Then we define the decay day in a similar fashion as the last day as part of a blocking episode before 4 days without blocking. This procedure yields 106 onset days from which the duration is measured. The majority of SSA blocking events last 4 or 5 days (31% and 19%, respectively). Then the number of blocking events gradually decreases as the duration increases up to 12 days. After that, there are two 15-day events and one 18-day event. Most striking is the persistent event that lasts 30 consecutive days starting on 15 January 2014. Its impact will be discussed separately in section 4.

The general behavior of the SSA blocking events is investigated now by plotting composites of various fields

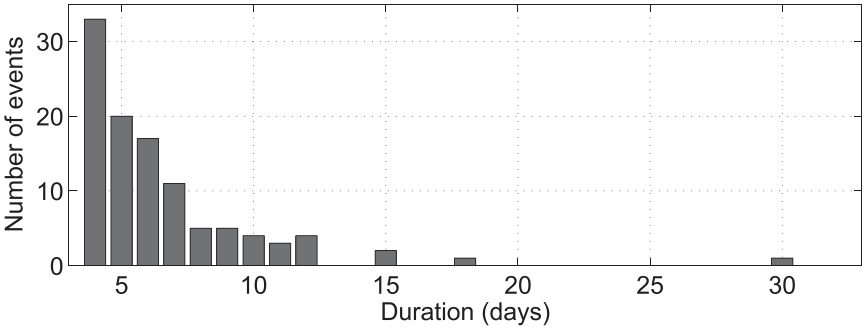

FIG. 4. Number of SSA blocking events in DJFM for the period of 1979–2014 lasting at least a given number of days (duration). The total number of events is 106.

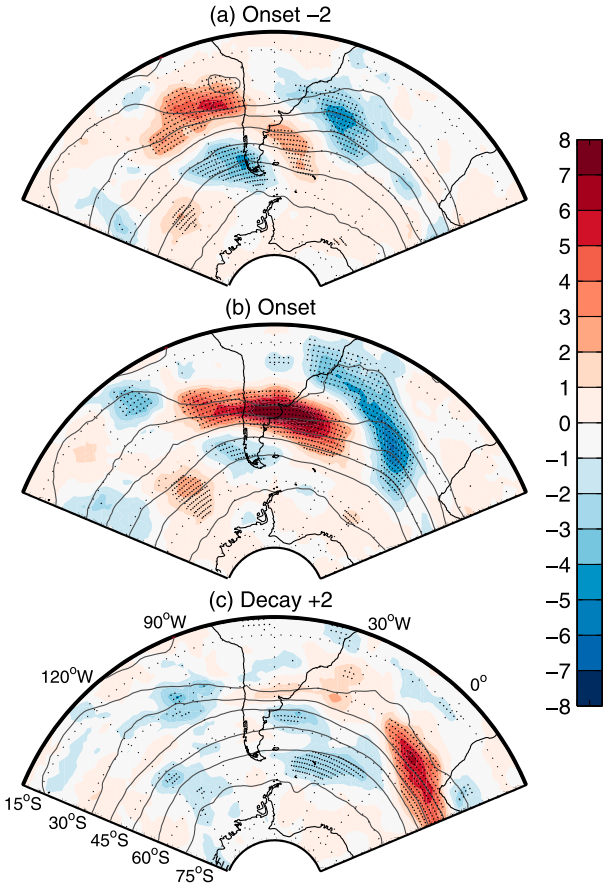

FIG. 5. Composites of anomalies (shading) and full field (contours) of potential temperature on the tropopause (−2 PVU surface) for the SSA blocking events in DJFM: (a) 2 days before the onset day, (b) on the onset day, and (c) 2 days after the decay day. There are 106 onset and decay days. Contour interval is every 10 K starting from 310 K (southern contour). Gray dots indicate areas where the composites are statistically significant different from the climatology at 95% confidence level.

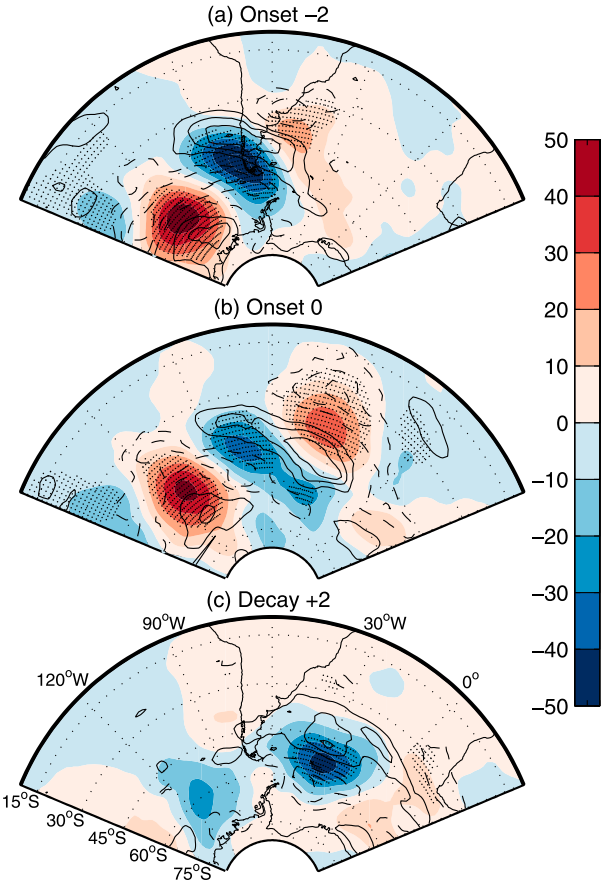

FIG. 6. Composites of geopotential height anomalies at 500 hPa (shading; m) and zonal wind speed anomalies at 500 hPa (contours; m s^{-1}) for the SSA blocking events in DJFM: (a) 2 days before the onset day, (b) on the onset day, and (c) 2 days after the decay day. Contour interval is 1 m s^{-1} with negative contours dashed and the zero contour omitted; only statistically significant contours are plotted. Gray dots indicate areas where the composites of geopotential height anomalies are statistically significantly different from the climatology at 95% confidence level.

on the onset day, 2 days before onset and 2 days after the decay day. The statistical significance of the composites is evaluated using a Monte Carlo test, randomly selecting the same number of blocking days from the climatological sample. This process is repeated 10 000 times and grid points where the composite mean is in the most extreme 5% of the surrogate composite mean are considered significant. The temporal evolution of the wave breaking is shown through the composites of potential temperature on the tropopause (Fig. 5). First inspection shows that the morphology of the SSA wave breaking is anticyclonic (anticlockwise); that is, cold air moves equatorward and westward (negative values in blue) to the east of warm air that moves poleward and eastward (positive values in red). The anomalies are strongest on the onset day with the boundary between the two air masses intersecting the South American coast north of 30°S; they are practically absent two days after the decay day. The full field (contours) shows prominent bending of the 360-K isentrope on the onset day. While individual events are constrained to exhibit a large-scale reversal of the meridional gradient, as in the example in Fig. 1, the picture is smoothed in Fig. 5 by compositing events from slightly different positions.

The cyclonic anomalies on the equatorward side of the wave breaking (not shown) disappear in the midtroposphere where positive geopotential height anomalies dominate, centered at 40°S and 40°W on the onset day (shading in Fig. 6). This is similar to the Eurasian blocking events described in Masato et al. (2012). The wave-breaking pattern causes an intensification of the westerly jet between the aforementioned positive

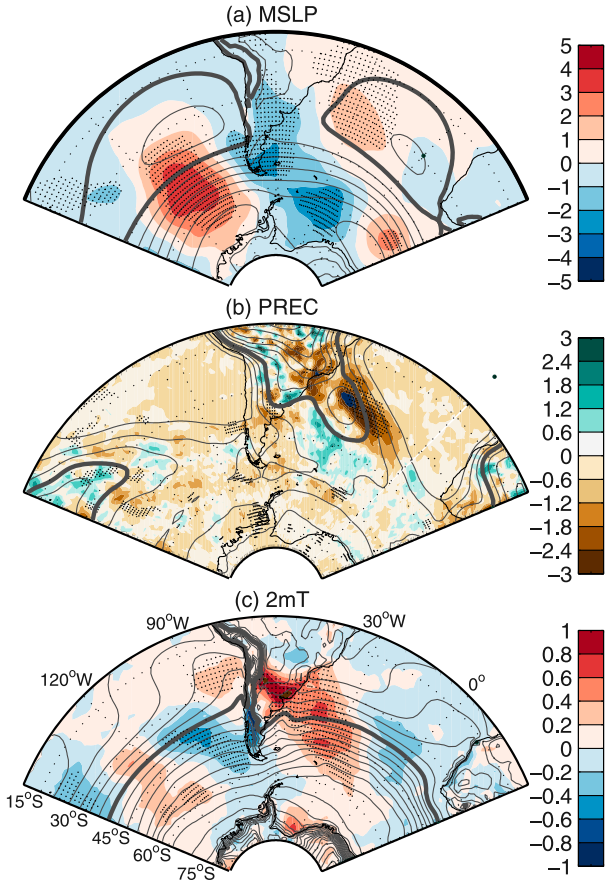

FIG. 7. Composites of anomalies of (a) MSLP, (b) precipitation, and (c) temperature at 2 m, for the SSA blocking events in DJFM on the onset day (shading). The contours display the climatological mean. In (a)–(c), contour intervals are every 5 hPa, 1 mm day^{-1}, and 2 K, respectively; bold lines are 1015 hPa, 4 mm day^{-1}, and 290 K, respectively. Gray dots indicate areas where the composites are statistically significantly different from the climatology at 95% confidence level.

geopotential height anomalies and the negative anomalies over the tip of South America (solid contours in Fig. 6b). Note that the mean position of the jet at this time of the year is around 44°S (Fig. 3). Before and after the blocking, changes in the jet over the SSA region are not significant, but the incoming wave prior to blocking onset is clear (Figs. 6a,c).

The impacts of SSA blocking on the mean sea level pressure (MSLP), precipitation, and air temperature at 2 m are now analyzed for the onset day (Fig. 7). The spatial pattern of MSLP is very similar to that of geopotential height at 500 hPa with positive anomalies over eastern South America and the South Atlantic (cf. Figs. 7a and 6b). The South Atlantic subtropical high is displaced to the west when compared to its climatological position (represented by the bold contour in Fig. 7a). As a

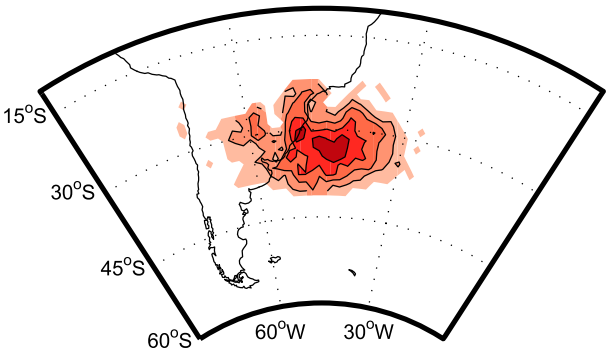

FIG. 8. Percentage of warm temperature extremes (defined as 99th percentile) occurring simultaneously with SSA blocking for each grid point. Contour interval is every 10% starting from 50%. Grid points are masked in white when the relationship is not statistically significant at the 99% confidence level.

consequence, convection is prevented and precipitation is deficient over a band oriented northwest–southeast, from southeast Brazil toward the western South Atlantic (Fig. 7b). This practically coincides with the position of the SACZ and suggests that blocking episodes can prevent the development of the SACZ. The negative anomalies of precipitation reach 3 mm day^{-1}, which is a similar order of magnitude to the climatology there (the bold contour in Fig. 7b represents 4 mm day^{-1}).

In addition, there is an increase in surface air temperature over the area where midtroposphere positive geopotential height anomalies dominate (Fig. 7c). This is probably due to the subsidence and lack of cloud cover associated with the blocking. The temperature anomalies are relatively weak reaching only 1 K. Nevertheless they are statistically significant. The impact of blocking on the surface temperature becomes more evident when we look at temperature extremes. We calculate the percentage of days in which temperature extremes (above the 99th percentile) occur simultaneously with SSA blocking for each grid point (Fig. 8). The association of SSA blocking to temperature extremes is clear: between 50% and 80% of warm temperature extremes over southeast Brazil occur during SSA blocking days.

In summary, we find that the SSA events exhibit a clear signature of large-scale wave breaking on the tropopause. The associated reversal of the meridional gradient in potential temperature is relatively shallow, but the events are nevertheless associated with anticyclonic flow through the depth of the troposphere and significant anomalies in surface temperature and precipitation. The position of the blocking varies for the different individual events and this can explain the weak anomalies shown in the composites. The individual events used to construct the composites have similar

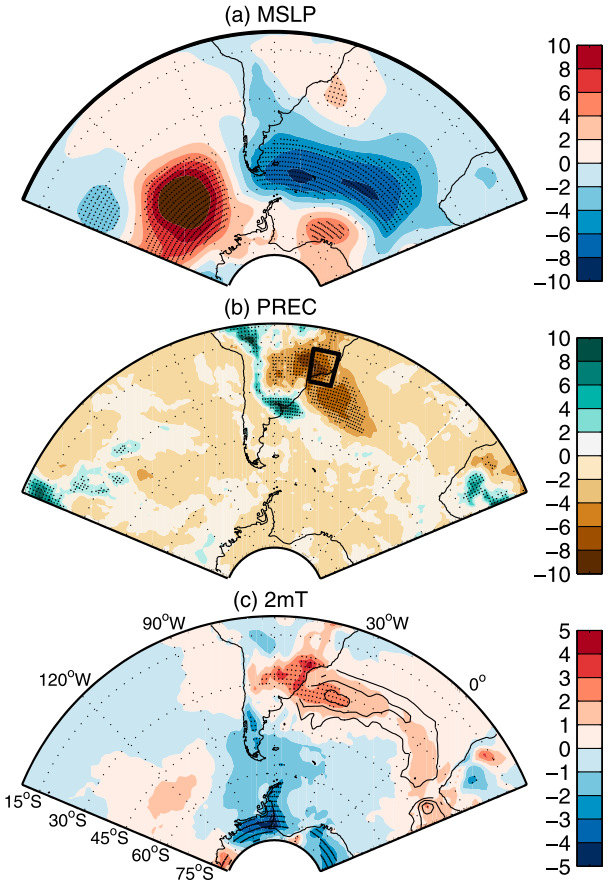

FIG. 9. As in Fig. 7, but for the 2014 event (15 Jan–13 Feb 2014) without the climatological means. Box in (b) encompasses southeast Brazil (16°–26°S, 40°–48°W), where precipitation is averaged to produce the time series discussed in the text. Contours in (c) show SST anomalies in the South Atlantic (isotherms of 1°, 2°, and 3°C).

features but larger amplitudes, as we shall see in the next section for the summer of 2013/14 (Fig. 9).

4. The summer of 2013/14

Extreme events of temperature and precipitation are generally associated with persistent individual blocking events. In this section we focus on the summer of 2013/14, not only because it was unprecedentedly dry and warm but also because it featured a record number of blocking days (Figs. 9 and 10, respectively). The time series of the number of SSA blocking episode days per summer (DJFM) shows that there were 50 blocking days during the summer of 2013/14 (solid black line in Fig. 10a). This value is above three standard deviations (solid black line in Fig. 10b). Moreover, one event lasted 30 days from 15 January 2014 (shown in Fig. 1) to 13 February 2014. To put this in context, the second longest event in the period considered in this study lasted 18 days (Fig. 4).

The impact of persistent blocking on the surface can be seen clearly in Fig. 9. The pattern of MSLP is similar to that obtained from the composite of all events, displaying a wave pattern with negative anomalies over the tip of South America and positive anomalies over the SSA region (cf. Figs. 7a and 9a). The amplitude of the MSLP anomalies is, however, slightly larger, reaching up to +4 hPa near the SSA region. It is also clear that this persistent event led to deficient rainfall and surface warming in the SACZ area (Figs. 9b,c). The precipitation anomalies reach up to $-10\,\mathrm{mm\,day^{-1}}$ with temperatures 5 K higher than the mean in southeast Brazil (box in Fig. 9b). Moreover, daily precipitation averaged over southeast Brazil (box in Fig. 9b) was below the climatological mean during 95% of the time and below one standard deviation during 75% of the time (considering the entire 30-day episode). It is noteworthy that the second- and third-worst droughts in southeast Brazil also occur during years with a very high number of blocking days, respectively in 1984 and 2001. The latter was responsible for a widespread shortage of energy in Brazil (Drumond and Ambrizzi 2005). In addition to the dry anomalies, Fig. 9b shows that SSA blocking leads to excess rainfall over the neighboring Amazon, Uruguay, Paraguay, and northern Argentina regions, at least for persistent events like the summer of 2013/14. In southern South America, this might be due to the fact that anticyclonic system blocks the equatorward propagation of cold fronts that otherwise would help the establishment of the SACZ over southeast Brazil (Nieto-Ferreira et al. 2011). The cold fronts suddenly stall and become stationary over southern South America, causing the excess precipitation there.

Note that the positive MSLP anomalies over the SSA area are not statistically significant for this persistent event. This is probably due to the fact that the heating near the ground can lead to the formation of a cyclonic thermal low with opposite near-surface circulation (Fischer et al. 2007). For this reason, Pfahl and Wernli (2012) suggest that atmospheric blocking in the middle to upper troposphere is a better predictor of surface warm and dry extremes. Moreover, the surface warming is collocated with the region of anticyclonic circulation in the upper-middle troposphere (not shown) and deficient rainfall (Fig. 9b), suggesting that the subsidence and clear-sky radiative forcing are responsible for the warming rather than the advection of warm air, which is weak over this area (Pfahl and Wernli 2012; Stefanon et al. 2012).

Our results also corroborate the suggestion by Pfahl and Wernli (2012) that the duration of the event is crucial for the extreme warm conditions over land due to its role in the depletion of soil moisture and an

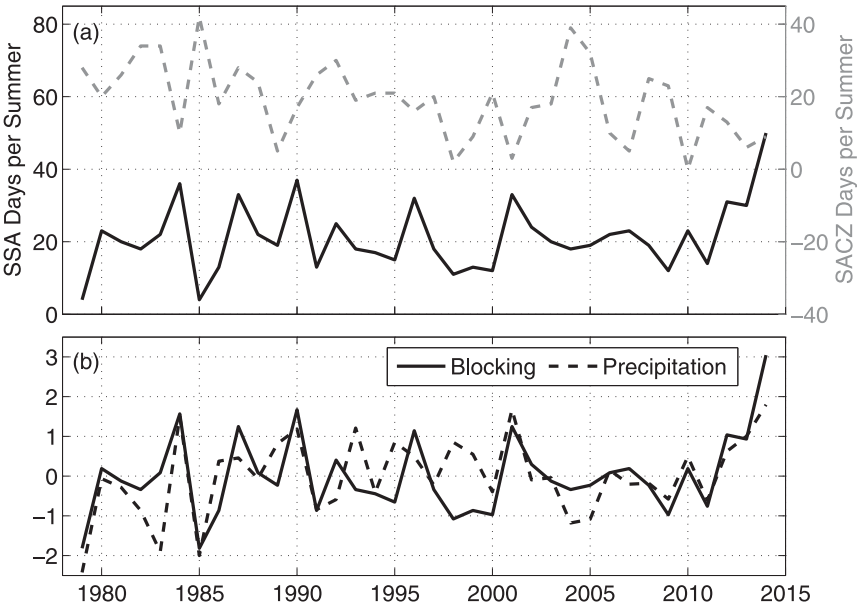

FIG. 10. Time series of SSA blocking (solid black) and SACZ (dashed gray) days per summer (DJFM) for the period of 1979–2014 (depicted are the years referent to JFM). They are statistically anticorrelated at the 95% confidence level (−0.37). (b) Time series of SSA blocking (solid black) and precipitation (dashed black) over southeast Brazil (box in Fig. 9b), normalized by their respective means and standard deviations. Note that the time series of precipitation is multiplied by −1 for easy comparison.

associated increase in sensible heat fluxes. Over the ocean, De Almeida et al. (2007) show that there is a negative thermodynamic feedback between the SACZ and the underlying SST anomalies over the western South Atlantic, in which the presence of clouds leads to a SST cooling and vice versa. Indeed for this persistent event, the lack of clouds leads to an increase in the SST of up to 3°C in the western South Atlantic, extending eastward along the basin (contours in Fig. 9c). This effect, however, is not observed when all blocking events are considered (not shown), emphasizing the importance of the duration of blocking.

5. Variability associated with the subtropical South America blocking

From previous sections, it has become clear that SSA blocking can lead to deficient rainfall and temperature extremes with devastating socioeconomic consequences. In addition, the number of SSA blocking episode days per summer varies greatly from year to year (Fig. 10). We now show that precipitation averaged over southeast Brazil (box in Fig. 9b) is anticorrelated to the number of SSA blocking days (Fig. 10b). The correlation coefficient is −0.65 for the period 1979–2014, which explains more than 40% of the variance. Note that in El Niño years the relationship between precipitation and the number of SSA blocking days breaks down, in particular for 1982/83, 1991/92, 1994/95, 1997/98, and 2004/05. As a consequence, the correlation between precipitation and SSA blocking deteriorated in the 1990s when El Niño events were more frequent. Excluding the 1990s, the correlation coefficients between the two time series are −0.78 and −0.86 for the periods of 1979–91 and 2000–14, respectively. Note that the time series of number SSA blocking days are not correlated to either El Niño–Southern Oscillation (ENSO) or the southern annular mode (SAM), the dominant modes of climate variability in the Southern Hemisphere.

To understand this relationship between SSA blocking and precipitation we need to understand the link between blocking and the SACZ based on our hypothesis that SSA blocking causes the persistent anticyclonic anomalies that can prevent the establishment of the SACZ, which in turn is the main source of rainfall over the SSA region during the summer. So presumably years with more blocking days coincide with years with fewer SACZ days and less precipitation. To define a SACZ event, we carry out an empirical orthogonal function (EOF) analysis on daily OLR anomalies over the region 35°S–0°, 80°–20°W that encompasses the SACZ (van der Wiel et al. 2015). Using a similar methodology to

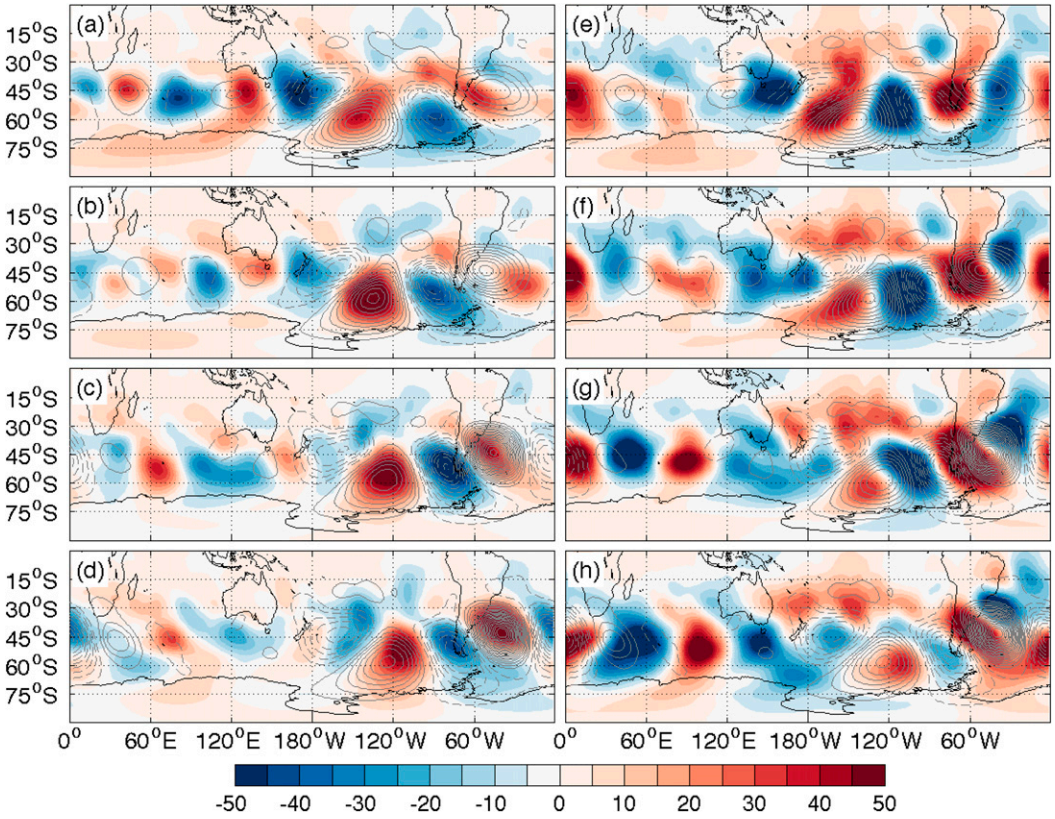

FIG. 11. Time-lagged composites of geopotential height anomalies at 200 hPa (shading; m) for the SSA blocking events in DJFM: (a) −6 days, (b) −4 days, (c) −2 days, and (d) onset day. (e)–(h) As in (a)–(d), but for SACZ events. Contours represent regression of geopotential height anomalies at 200 hPa over the SSA point (40°W, 40°S) against geopotential height anomalies at 200 hPa for DJFM at the same lags (every 10 m).

Matthews (2012) for the South Pacific convergence zone, an SACZ episode was defined when the principal component of the first leading mode exceeded +1 standard deviation and lasted for 4 days [instead of −5 and +5 days used by Matthews (2012) to be consistent with the blocking index methodology]. The correlation coefficient between the time series of precipitation and that of SACZ episode days per summer is +0.75, implying that the SACZ explains more than 50% of precipitation variability in the summer. The time series of SACZ episode days per summer is statistically significantly anticorrelated to that of SSA blocking, with a correlation coefficient of −0.37 (gray and black lines, respectively, in Fig. 10a). Again, El Niño events degrade this relationship; excluding the 1990s, the correlation coefficient is −0.48 and −0.52 for the periods of 1979–91 and 2000–14, respectively.

It is also important to investigate what differentiates years with more SSA blocking days (and fewer SACZ events) from those years with fewer blocking days (and more SACZ events). We begin by analyzing the period prior to wave breaking to identify any consistent precursors. We compare time-lagged composites of geopotential height anomalies at 200 hPa over the 6 days prior to the onset of blocking episodes to those for SACZ episodes (Fig. 11). A Rossby wave packet propagates eastward along the jet from the Indian Ocean to the tip of South America, where it is refracted equatorward (Figs. 11a–d). In the SACZ composites, in contrast, the wave packet seems to originate in the Pacific and not in the Indian Ocean (Figs. 11e–h). The anomalies of geopotential height over the Indian Ocean are not as coherent to those over the Pacific Ocean for the SACZ case (Fig. 11e) as they are for the SSA case (Fig. 11a). The contour lines in Fig. 11 show lagged regressions of the height anomalies against the height over the SSA region using all summer days from the 1979–2014 period. The resulting wave train is very similar to the SSA composite, underscoring that this is the dominant precursor to SSA variability. Moreover, the signal over the Indian Ocean that appears in the regression contours at −6 lags coincides solely with the anomalies for the SSA case (cf. Figs. 11a,e).

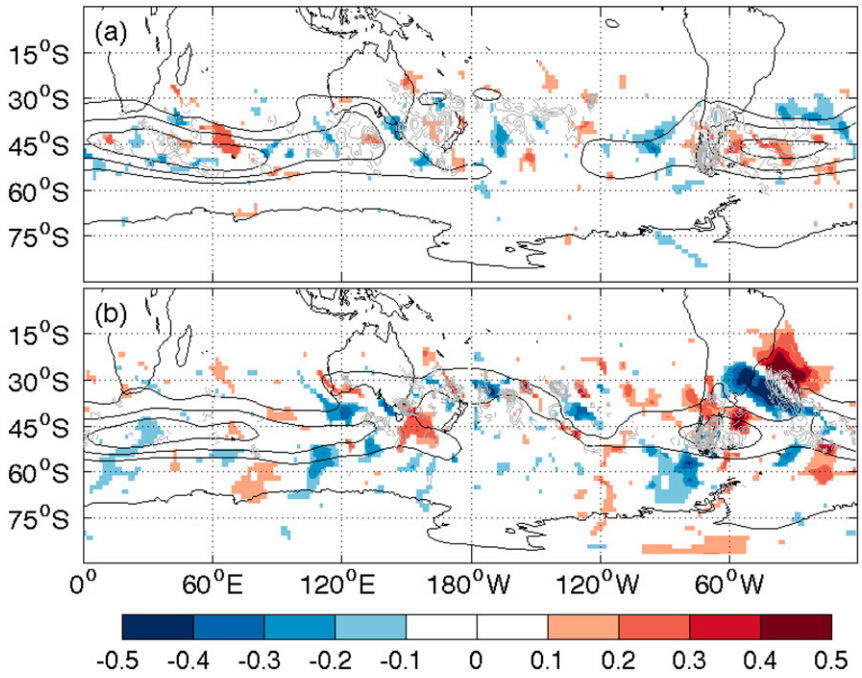

FIG. 12. Rossby wave source (shading; $10^{-9}\,s^{-2}$), standard deviation of Rossby wave source (gray contours above $1 \times 10^{-9}\,s^{-2}$; $0.1 \times 10^{-9}\,s^{-2}$ contour interval), and isotachs of 200-hPa zonal wind (black contours above $25\,m\,s^{-1}$; $5\,m\,s^{-1}$ contour interval) for (a) SSA blocking events and (b) SACZ events.

To help us to identify the source of variability, we also calculate the Rossby wave source (RWS) for both cases, using the formulation by Sardeshmukh and Hoskins (1988). The RWS is defined as $-\nabla\cdot(v_\chi\cdot\zeta)$, where v_χ is the divergent component of the horizontal velocity field at 200 hPa and ζ is the absolute vorticity. The RWS can be used to examine the mechanisms by which the midlatitude circulation responds to changes associated with tropical convection. The RWS is largest in regions where divergent winds and gradients in absolute vorticity are largest. Therefore, a strong RWS occurs in the jet stream regions where large gradients in vorticity occur poleward of diabatic tropical heating. These regions are the locations of wave train excitation. Color shading in Fig. 12 shows the RWS averaged over a 6-day period prior to the onset for both cases. Indeed, a strong RWS is present in the Indian Ocean for the SSA blocking case and over the western Pacific (between Australia and New Zealand sector) for the SACZ case (values above $0.2 \times 10^{-9}\,s^{-2}$). We also show the standard deviation of Rossby wave source (gray contours in Fig. 12), which can be interpreted as an estimate of the intraseasonal variability. Again Rossby wave source is very active along the jet core in the Indian Ocean only for the SSA blocking case (Fig. 12a), suggesting that variability in that sector (associated with tropical convection as we shall see in next section) can excite fluctuations resembling the wave pattern shown in Figs. 11a–d. In other words, the strong jet structure provides a strong background vorticity gradient, forming the strongest RWS area. For the SACZ case, the Rossby wave source activity is concentrated in the Pacific Ocean (Fig. 12b), which is more consistent with the seasonal mean for austral summer [see Figs. 14a,b from Ding et al. (2012)]. More recently, O'Kane et al. (2016) have shown that the Indian Ocean midlatitudes are also an important source of Rossby waves in the summer and autumn.

Note that since the SSA blocking events are by definition events of Rossby wave breaking over South America, we see very little propagation beyond South America. In contrast, the SACZ wave packet does not break over South America. This is consistent with the work of van der Wiel et al. (2015), who showed continued propagation of the SACZ wave over the region. Moreover, convection associated with SACZ is likely to trigger more wave activity downstream. Indeed, the geopotential height anomalies are more intense and propagate around the globe for the SACZ composites (Fig. 11). This also explains more global RWS activity for the SACZ case (Fig. 12). Thus the impacts of the SACZ go beyond South America. Grimm and Reason (2015) have shown, for instance, that convection over South America affects

southern African rainfall, while Reeder et al. (2015) have shown that Rossby waves originating in South America can lead to extreme summertime cold fronts associated with the most catastrophic bush fires in Australia.

The regression pattern also serves as a marker against which to highlight differences between the SSA and SACZ composites. For example, color contours in Fig. 11 show that the refraction pattern of the wave packet over the tip of South America is different, in particular on the onset day. For both cases, the amplitude of the wave packet increases and at the same time its wavelength decreases, consistent with Rossby wave propagation theory (Webster and Chang 1998). However, the refraction path is different with the SSA wave packet propagating toward the South Atlantic while the one associated with the SACZ propagates more aligned with the east coast of South America. This is due to the distinct locations of the jet exit ($\partial u/\partial x < 0$) over the southwestern South Atlantic for both cases (black contours in Fig. 12). The jet exit is closer to South America for the SACZ case. It is also clear that the jet is stronger over the east Atlantic–Indian Ocean sector in both cases, explaining the absence of wave breaking in this sector (Fig. 2). In addition, the phase differs between the two cases. For example, the SSA blocking composite at day −2 features positive geopotential height anomalies over the Amundsen Sea followed by negative anomalies over the tip of South America and positive anomalies over the SSA region. The opposite is true for the SACZ composite (Fig. 11). Although there is a phase shift of about half their wavelengths, with the length of SACZ wave is shorter than that of the SSA wave. This is due to the fact that for the SACZ the jet exit is closer to the tip of South America. The work by Webster and Chang (1998) on Rossby wave propagation in a heterogeneous zonal flow shows that when $\partial u/\partial x < 0$, the wavenumber increases (wavelength decreases) along a ray. As the wavenumber increases, the longitudinal group speed will decrease and wave energy density will increase [for a detailed discussion see Widlansky et al. (2011)]. Thus, the SACZ wave has a shorter length and larger group velocity (explaining the phase shift). Widlansky et al. (2011) showed for the South Pacific that where the wave group velocity is reduced, the wave energy locally increases, resulting in a highly energetic convective region that develops oriented diagonally away from the equator. This is consistent with our results for SACZ.

6. Tropical precursor to the subtropical South America blocking

We now need to investigate what triggers the different wave patterns we have seen in the previous section. It is important to know if there is a precursor to SSA blocking and/or to the SACZ in order to improve our capability of predicting rainfall over this area. Earlier studies have shown that the SACZ variability is associated with the MJO (Kousky and Kayano 1994; Jones and Carvalho 2002; Carvalho et al. 2004). In particular, Carvalho et al. (2004) show that SACZ events lasting longer than 3 days are modulated by the MJO, mainly when convection is prominent over the western/central Pacific and suppressed over the Maritime Continent. MJO convection triggers the so-called Matsuno–Gill response serving as a wave source for poleward propagation of Rossby waves in both hemispheres (Matsuno 1966; Gill 1980). In particular, it has been well documented that the MJO can trigger an extratropical wave train that resembles the Pacific–North American teleconnection pattern (Adames and Wallace 2014, and references therein). Moreover, the MJO has been linked to blocking in the Northern Hemisphere (Moore et al. 2010; Hamill and Kiladis 2014; Henderson et al. 2016).

The MJO is therefore a likely candidate to be a precursor to SSA blocking. Given the apparent difference in wave origin in Figs. 11 and 12, it is possible that convection over the Indian Ocean associated with MJO phases 1 and 2 could trigger the wave train that leads to SSA blocking, whereas convection over the western/central Pacific associated with phases 6 and 7 is more likely to lead to SACZ events. The latter resembles the Pacific–South American teleconnection pattern (Mo and Paegle 2001). To test this hypothesis, we have performed a maximum covariance analysis (MCA) of daily OLR anomalies over the tropical belt (30°N–30°S) and geopotential height anomalies at 200 hPa over the area surrounding South America (0°–150°W, 0°–90°S) for all summers (DJFM) for the period 1979–2014 (Bretherton et al. 1992). The MCA provides the dominant spatial patterns of covariability between the two fields. The leading mode is associated with ENSO (not shown) accounting for 12% of the squared covariance. For the second mode (Fig. 13), enhanced convection over the Indian Ocean (negative values of OLR) and suppressed convection over the Pacific (positive values of OLR) occur in association with a Rossby wave train pattern similar to that associated with the SSA blocking. The advection of planetary vorticity by the divergent, upper-tropospheric outflow from the enhanced convection in the Indian Ocean excites the SSA Rossby wave train pattern, consistent with the RWS analysis (Fig. 12a). The OLR pattern resembles MJO phases 1 and 2. The second mode explains 8% of the covariance but is well separated from the remaining modes (Fig. 13b). Moreover, the time series of the second mode (not shown) is significantly correlated to those of SSA

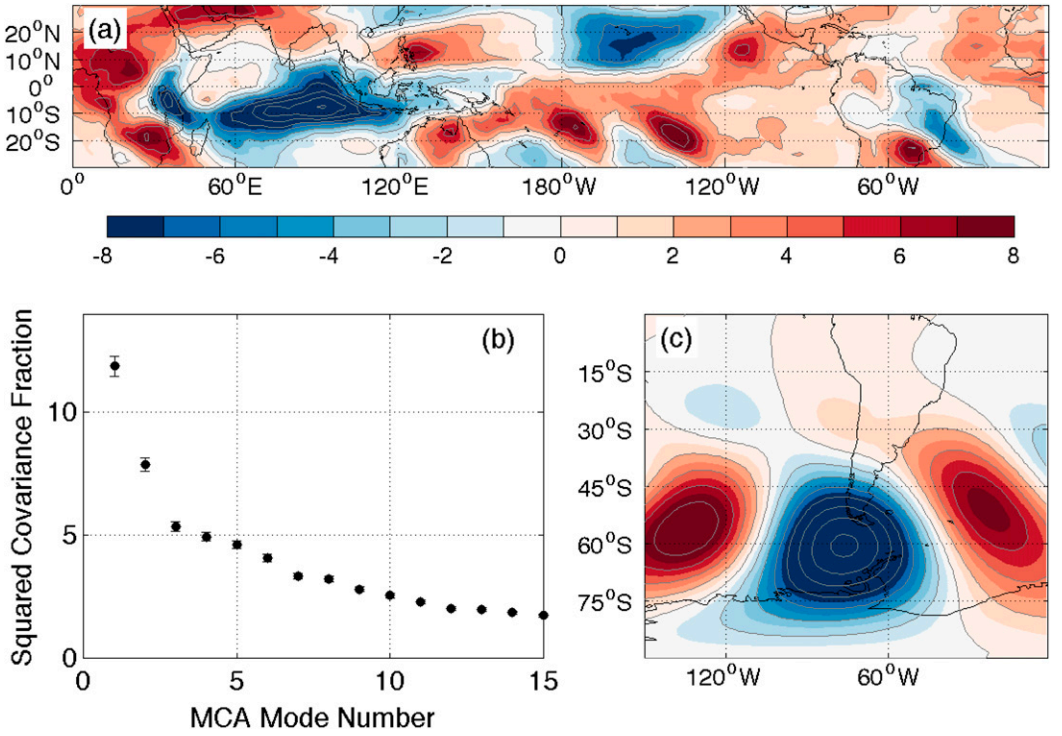

FIG. 13. The second mode patterns from the MCA of (a) OLR and (c) geopotential height at 200 hPa. The contour intervals are every 1 W m^{-2} in (a) and 100 m in (c). (b) The squared covariance fraction of the first 15 modes.

blocking days and precipitation, with correlation coefficients of 0.40 and −0.38, respectively.

To confirm that the MJO influences SSA blocking we now compute SSA blocking frequencies for each MJO phase by taking the number of blocked days during a given MJO phase at 0 lag divided by the total number of days within that MJO phase (Fig. 14). This methodology was based on Henderson et al. (2016). Here we use the MJO index by Kiladis et al. (2014) because it is computed from OLR data only, which is recommended when the convection signal is of primary interest. Figure 14 suggests that SSA blocking frequency increases during MJO phases 1, 2 (in the west of our region), and 5, when convection is mainly over the African continent and Indian Ocean and to a lesser extent over the Maritime Continent; and it decreases in phases 4, 6, and 7 when convection is over the western and central Pacific (although, the decrease in blocking frequency for phases 4, 6, and 7 is not statistically significant). We speculate that MJO phases 1, 2, and 5 trigger Rossby wave trains with the same phase that leads to SSA blocking, whereas MJO phases 4, 6, and 7 trigger Rossby wave trains with the phases that enhance SACZ. We have also performed the same analysis except with MJO leading at 6-, 4-, and 2-day lags and found similar results for the SSA region (not shown). We also note in passing that Fig. 14 demonstrates that the MJO clearly modulates blocking activity at many other locations around the Southern Hemisphere.

Finally, computing the time series of SSA blocking episode days per summer excluding those days when blocking occurs simultaneously with MJO phases 1 and 2 shows a strong reduction in the number of blocking days (Fig. 15a). From a total of 624 blocking days in DJF, 343 days occur during phases 1 and 2, representing 55% of blocking days. The long-term variability in blocking is also reduced, for example in the period of increasing blocking occurrence in 2000–14. As a part of this, the extreme seasons are strongly affected, with no summers exceeding 20 days of blocking once these MJO phases are discounted. Here we have used DJF because the changes in frequency of MJO days per phase between the periods of 1979–99 and 2000–14 are more evident in DJF, as is the increase in blocking occurrence during the period of 2000–14 (cf. Figs. 10a and 15a).

This long-term modulation is consistent with the results by Seth et al. (2015), who showed a relationship between the precipitation over the southeast Brazil and the interdecadal Pacific oscillation (IPO). A negative phase of the IPO is generally associated with a strengthening of the trade winds over the Pacific that

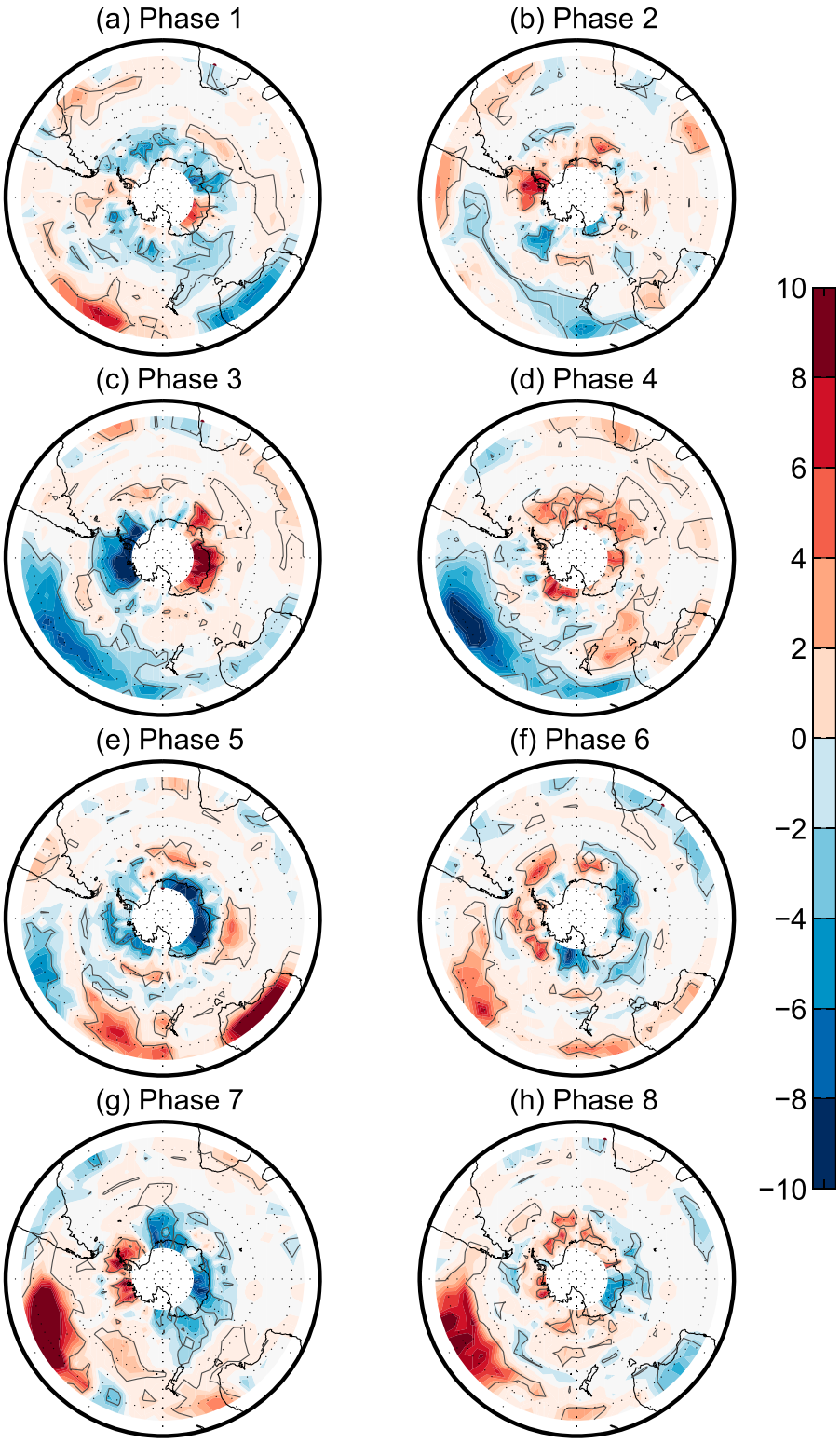

FIG. 14. SSA blocking frequency anomalies defined as deviations from DJFM mean (from Fig. 2) for each phase of the MJO. Contours encompass areas where the anomalies are statistically significant at the 95% confidence level using a Monte Carlo test in which seasons are shuffled randomly with a sample size of 10 000, similar to Scherrer et al.'s (2006) methodology.

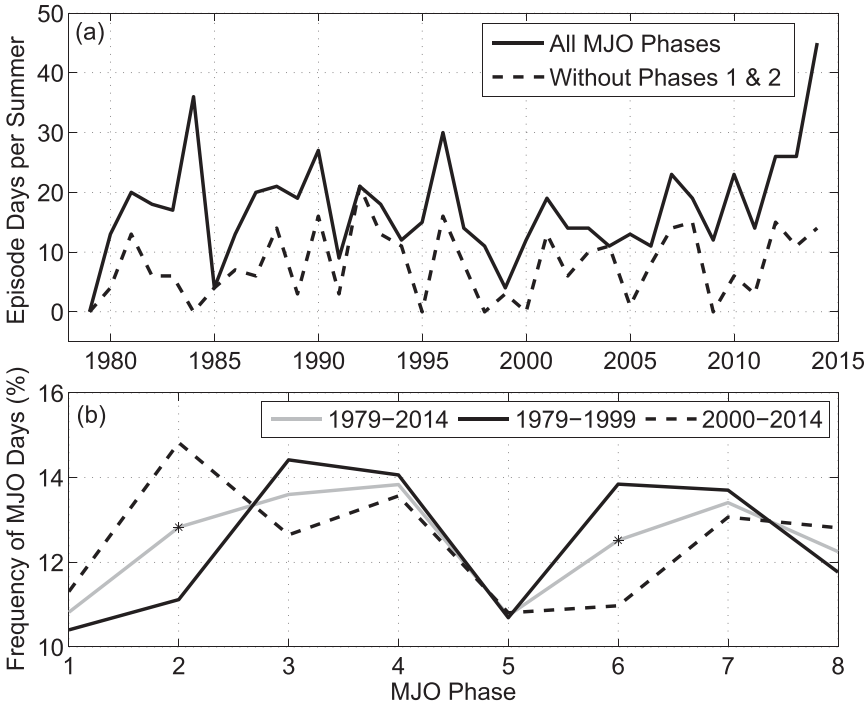

FIG. 15. (a) Time series of total number of SSA blocking episode days per summer (DJF) for the period of 1979–2014 (solid line) and excluding those days when blocking occurs simultaneously with MJO phases 1 and 2 (dashed line). (b) Frequency of MJO days per phase for 1979–2014, 1979–99 (positive IPO), and 2000–14 (negative IPO). Asterisks represent phases when the differences are statistically significant at the 95% confidence level.

leads to a La Niña–like state with cooling of the tropical Pacific (England et al. 2014). This mechanism is also believed to lead indirectly to a warming of the tropical Indian Ocean (Lee et al. 2015). We also know that the MJO tends to occur during neutral and weak La Niña years (Hendon et al. 1999; Zhang 2005). We speculate that in the last decade or so (2000–14) of negative IPO, with cooler Pacific and warmer Indian Ocean temperatures, convection would have been enhanced over the Indian Ocean and suppressed over the Pacific. (The phase of the IPO changed from positive to negative in 1999–2000.) The MJO would have been more active, with more days during phases 1 and 2 and fewer days during phases 6 and 7, which is indeed the case (Fig. 15b). As a consequence, SSA blocking days have become increasingly more frequent in the last decade and SACZ events less so.

7. Summary and conclusions

In this study we have examined wave-breaking events over the subtropical South American–South Atlantic sector during austral summer following Berrisford et al. (2007). We find that although the reversal of the meridional gradient of potential temperature on the tropopause is relatively shallow, the events are nevertheless associated with anticyclonic flow through the upper-middle troposphere and significant anomalies in surface temperature and precipitation. We therefore refer to these low-latitude wave-breaking events as SSA blocking events, even though they do not divert or block the midlatitude westerly flow.

The tropopause-level, PV-based methodology used here is proven to be a reliable tool to determine blocking events that lead to extremes of surface temperature and precipitation. Up to 80% of warm surface air temperature extremes occur simultaneously with SSA blocking events. The frequency of SSA blocking days is highly anticorrelated to the rainfall over southeast Brazil. The worst droughts in this area during the summers of 1984, 2001, and 2014 are linked to record number of SSA blocking days. The persistence of these events (i.e., with many consecutive days of blocking) is also important to generate the extremes.

We have shown that the SSA blocking can prevent the establishment of the SACZ. As such, years with more blocking days coincide with years with fewer SACZ days and less precipitation. Convection mainly over the

Indian Ocean associated with MJO phases 1 and 2 can trigger the wave train that leads to SSA blocking whereas convection over the western/central Pacific associated with phases 6 and 7 is more likely to lead to SACZ events. We find that the MJO modulates the long-term variability of SSA blocking frequency.

The wave packets associated with SSA blocking and SACZ episodes differ not only in their origin but also in their phase and refraction pattern. The SSA wave packet propagates toward the South Atlantic whereas the propagation of the SACZ wave packet is more aligned to the South American coast. This is due to the location of the jet exit, with the latter being closer to the tip of South America. Close to the onset day, positive geopotential height anomalies occur over the Amundsen Sea followed by negative anomalies over the tip of South America and positive anomalies over the SSA, leading to anticyclonic flow over this region. In contrast, the phase of the SACZ wave packet is reversed, with negative geopotential anomalies and thus cyclonic circulation over the SSA area. This circulation pattern is typical of the South America monsoon system, when the establishment of the SACZ leads to abundant summer rainfall.

Further work is needed to understand in more detail the mechanisms involved in the relationship between MJO and SSA blocking and also why El Niño events degrade the relationship between SSA blocking frequency and precipitation over southeast Brazil. Previous studies have shown that MJO can enhance predictability in the Northern Hemisphere subtropics and extratropics (Cassou 2008; Hamill and Kiladis 2014). However, this has not been explored for South America.

Acknowledgments. This work has been supported by CNPq (Grant 232480/2014-1) and is part of the research conducted by the INCT-MC, INCT-Mar COI, and Rede CLIMA. The ERA-Interim reanalysis dataset was provided by ECMWF. NOAA/OAR/ESRL PSD provided GPCP, OISST, and interpolated OLR and OLR MJO index datasets.

REFERENCES

Adames, Á. F., and J. M. Wallace, 2014: Three-dimensional structure and evolution of the MJO and its relation to the mean flow. *J. Atmos. Sci.*, **71**, 2007–2026, doi:10.1175/JAS-D-13-0254.1.

Barnes, E. A., J. Slingo, and T. Woollings, 2012: A methodology for the comparison of blocking climatologies across indices, models and climate scenarios. *Climate Dyn.*, **38**, 2467–2481, doi:10.1007/s00382-011-1243-6.

Barriopedro, D., R. García-Herrera, and R. M. Trigo, 2010: Application of blocking diagnosis methods to general circulation models. Part I: A novel detection scheme. *Climate Dyn.*, **35**, 1373–1391, doi:10.1007/s00382-010-0767-5.

Berrisford, P., B. J. Hoskins, and E. Tyrlis, 2007: Blocking and Rossby wave breaking on the dynamical tropopause in the Southern Hemisphere. *J. Atmos. Sci.*, **64**, 2881–2898, doi:10.1175/JAS3984.1.

Bretherton, C. S., C. Smith, and J. M. Wallace, 1992: An intercomparison of methods for finding coupled patterns in climate data. *J. Climate*, **5**, 541–560, doi:10.1175/1520-0442(1992)005<0541:AIOMFF>2.0.CO;2.

Buehler, T., C. C. Raible, and T. F. Stocker, 2011: The relationship of winter season North Atlantic blocking frequencies to extreme cold or dry spells in the ERA-40. *Tellus*, **63A**, 212–222, doi:10.1111/j.1600-0870.2010.00492.x.

Carvalho, L. M. V., C. Jones, and B. Liebmann, 2002: Extreme precipitation events in southeastern South America and large-scale convective patterns in the South Atlantic convergence zone. *J. Climate*, **15**, 2377–2394, doi:10.1175/1520-0442(2002)015<2377:EPEISS>2.0.CO;2.

——, ——, and ——, 2004: The South Atlantic convergence zone: Intensity, form, persistence, and relationships with intraseasonal to interannual activity and extreme rainfall. *J. Climate*, **17**, 88–108, doi:10.1175/1520-0442(2004)017<0088:TSACZI>2.0.CO;2.

Cassou, C., 2008: Intraseasonal interaction between the Madden–Julian Oscillation and the North Atlantic Oscillation. *Nature*, **455**, 523–527, doi:10.1038/nature07286.

Coelho, C. A., and Coauthors, 2016a: The 2014 southeast Brazil austral summer drought: Regional-scale mechanisms and teleconnections. *Climate Dyn.*, **46**, 3737–3752, doi:10.1007/s00382-015-2800-1.

——, D. H. F. Cardoso, and M. A. F. Firpo, 2016b: Precipitation diagnostics of an exceptionally dry event in São Paulo, Brazil. *Theor. Appl. Climatol.*, **125**, 769–784, doi:10.1007/s00704-015-1540-9.

Damião Mendes, M. C. D., and I. F. A. Cavalcanti, 2014: The relationship between the Antarctic oscillation and blocking events over the South Pacific and Atlantic Oceans. *Int. J. Climatol.*, **34**, 529–544, doi:10.1002/joc.3729.

Davini, P., C. Cagnazzo, S. Gualdi, and A. Navarra, 2012: Bidimensional diagnostics, variability, and trends of Northern Hemisphere blocking. *J. Climate*, **25**, 6496–6509, doi:10.1175/JCLI-D-12-00032.1.

De Almeida, R. A. F., P. Nobre, R. J. Haarsma, and E. J. D. Campos, 2007: Negative ocean–atmosphere feedback in the South Atlantic convergence zone. *Geophys. Res. Lett.*, **34**, L18809, doi:10.1029/2007GL030401.

Dee, D. P., and Coauthors, 2011: The ERA-Interim reanalysis: Configuration and performance of the data assimilation system. *Quart. J. Roy. Meteor. Soc.*, **137**, 553–597, doi:10.1002/qj.828.

Ding, Q., E. J. Steig, D. S. Battisti, and J. M. Wallace, 2012: Influence of the tropics on the southern annular mode. *J. Climate*, **25**, 6330–6348, doi:10.1175/JCLI-D-11-00523.1.

Drumond, A. R. M., and T. Ambrizzi, 2005: The role of SST on the South American atmospheric circulation during January, February and March 2001. *Climate Dyn.*, **24**, 781–791, doi:10.1007/s00382-004-0472-3.

England, M. H., and Coauthors, 2014: Recent intensification of wind-driven circulation in the Pacific and the ongoing warming hiatus. *Nat. Climate Change*, **4**, 222–227, doi:10.1038/nclimate2106.

Fischer, E. M., S. I. Seneviratne, P. L. Vidale, D. Lüthi, and C. Schär, 2007: Soil moisture–atmosphere interactions during

the 2003 European summer heat wave. *J. Climate*, **20**, 5081–5099, doi:10.1175/JCLI4288.1.

Gabriel, A., and D. Peters, 2008: A diagnostic study of different types of Rossby wave breaking events in the northern extratropics. *J. Meteor. Soc. Japan*, **86**, 613–631, doi:10.2151/jmsj.86.613.

Gill, A. E., 1980: Some simple solutions for heat-induced tropical circulation. *Quart. J. Roy. Meteor. Soc.*, **106**, 447–462, doi:10.1002/qj.49710644905.

Gonzalez, P. L., and C. S. Vera, 2014: Summer precipitation variability over South America on long and short intraseasonal timescales. *Climate Dyn.*, **43**, 1993–2007, doi:10.1007/s00382-013-2023-2.

Grimm, A. M., and C. J. C. Reason, 2015: Intraseasonal teleconnections between South America and South Africa. *J. Climate*, **28**, 9489–9497, doi:10.1175/JCLI-D-15-0116.1.

Hamill, T. M., and G. N. Kiladis, 2014: Skill of the MJO and Northern Hemisphere blocking in GEFS medium-range reforecasts. *Mon. Wea. Rev.*, **142**, 868–885, doi:10.1175/MWR-D-13-00199.1.

Henderson, S. A., E. D. Maloney, and E. A. Barnes, 2016: The influence of the Madden–Julian oscillation on Northern Hemisphere winter blocking. *J. Climate*, **29**, 4597–4616, doi:10.1175/JCLI-D-15-0502.1.

Hendon, H. H., C. Zhang, and J. D. Glick, 1999: Interannual variation of the Madden–Julian oscillation during austral summer. *J. Climate*, **12**, 2538–2550, doi:10.1175/1520-0442(1999)012<2538:IVOTMJ>2.0.CO;2.

Huffman, G. J., R. F. Adler, M. Morrissey, D. T. Bolvin, S. Curtis, R. Joyce, B. McGavock, and J. Susskind, 2001: Global precipitation at one-degree daily resolution from multisatellite observations. *J. Hydrometeor.*, **2**, 36–50, doi:10.1175/1525-7541(2001)002<0036:GPAODD>2.0.CO;2.

Jones, C., and L. C. Carvalho, 2002: Active and break phases in the South American monsoon system. *J. Climate*, **15**, 905–914, doi:10.1175/1520-0442(2002)015<0905:AABPIT>2.0.CO;2.

Kiladis, G. N., J. Dias, K. H. Straub, M. C. Wheeler, S. N. Tulich, K. Kikuchi, K. M. Weickmann, and M. J. Ventrice, 2014: A comparison of OLR and circulation based indices for tracking the MJO. *Mon. Wea. Rev.*, **142**, 1697–1715, doi:10.1175/MWR-D-13-00301.1.

Kousky, V. E., and M. T. Kayano, 1994: Principal modes of outgoing longwave radiation and 250-mb circulation for the South American sector. *J. Climate*, **7**, 1131–1143, doi:10.1175/1520-0442(1994)007<1131:PMOOLR>2.0.CO;2.

Lee, S.-K., W. Park, M. O. Baringer, A. L. Gordon, B. Huber, and Y. Liu, 2015: Pacific origin of the abrupt increase in Indian Ocean heat content during the warming hiatus. *Nat. Geosci.*, **8**, 445–449, doi:10.1038/ngeo2438.

Liebmann, B., and C. A. Smith, 1996: Description of a complete (interpolated) outgoing longwave radiation dataset. *Bull. Amer. Meteor. Soc.*, **77**, 1275–1277.

——, G. N. Kiladis, J. A. Marengo, T. Ambrizzi, and J. D. Glick, 1999: Submonthly convective variability over South America and the South Atlantic convergence zone. *J. Climate*, **12**, 1877–1891, doi:10.1175/1520-0442(1999)012<1877:SCVOSA>2.0.CO;2.

——, ——, C. S. Vera, A. C. Saulo, and L. M. V. Carvalho, 2004: Subseasonal variations of rainfall in South America in the vicinity of the low-level jet east of the Andes and comparison to those in the South Atlantic convergence zone. *J. Climate*, **17**, 3829–3842, doi:10.1175/1520-0442(2004)017<3829:SVORIS>2.0.CO;2.

Madden, R., and P. Julian, 1994: Observations of the 40–50-day tropical oscillation—A review. *Mon. Wea. Rev.*, **122**, 814–837, doi:10.1175/1520-0493(1994)122<0814:OOTDTO>2.0.CO;2.

Marengo J. A., and Coauthors, 2012: Recent developments on the South American monsoon system. *Int. J. Climatol.*, **32**, 1–21, doi:10.1002/joc.2254.

Masato, G., B. J. Hoskins, and T. J. Woollings, 2009: Can the frequency of blocking be described by a red noise process? *J. Atmos. Sci.*, **66**, 2143–2149, doi:10.1175/2008JAS2907.1.

——, ——, and ——, 2012: Wave breaking characteristics of midlatitude blocking. *Quart. J. Roy. Meteor. Soc.*, **138**, 1285–1296, doi:10.1002/qj.990.

Matsuno, T., 1966: Quasi-geostrophic motions in the equatorial area. *J. Meteor. Soc. Japan*, **44**, 25–43.

Matthews, A. J., 2012: A multiscale framework for the origin and variability of the South Pacific convergence zone. *Quart. J. Roy. Meteor. Soc.*, **138**, 1165–1178, doi:10.1002/qj.1870.

Mo, K. C., and J. N. Paegle, 2001: The Pacific–South American modes and their downstream effects. *Int. J. Climatol.*, **21**, 1211–1229, doi:10.1002/joc.685.

Moore, R. W., O. Martius, and T. Spengler, 2010: The modulation of the subtropical and extratropical atmosphere in the Pacific basin in response to the Madden–Julian oscillation. *Mon. Wea. Rev.*, **138**, 2761–2779, doi:10.1175/2010MWR3194.1.

Nieto-Ferreira, R., T. M. Rickenbach, and E. A. Wright, 2011: The role of cold fronts in the onset of the monsoon season in the South Atlantic convergence zone. *Quart. J. Roy. Meteor. Soc.*, **137**, 908–922, doi:10.1002/qj.810.

Nogués-Paegle, J., and K. C. Mo, 1997: Alternating wet and dry conditions over South America during summer. *Mon. Wea. Rev.*, **125**, 279–291, doi:10.1175/1520-0493(1997)125<0279:AWADCO>2.0.CO;2.

O'Kane, T. J., J. S. Risbey, C. Franzke, I. Horenko, and D. P. Monselesan, 2013: Changes in the metastability of the midlatitude Southern Hemisphere circulation and the utility of nonstationary cluster analysis and split-flow blocking indices as diagnostic tools. *J. Atmos. Sci.*, **70**, 824–842, doi:10.1175/JAS-D-12-028.1.

——, ——, D. P. Monselesan, I. Horenko, and C. L. Franzke, 2016: On the dynamics of persistent states and their secular trends in the waveguides of the Southern Hemisphere troposphere. *Climate Dyn.*, **46**, 3567–3597, doi:10.1007/s00382-015-2786-8.

Oliveira, F. N., L. Carvalho, and T. Ambrizzi, 2014: A new climatology for Southern Hemisphere blockings in the winter and the combined effect of ENSO and SAM phases. *Int. J. Climatol.*, **34**, 1676–1692, doi:10.1002/joc.3795.

Parker, T. J., G. J. Berry, and M. J. Reeder, 2014: The structure and evolution of heatwaves over southeastern Australia. *J. Climate*, **27**, 5768–5785, doi:10.1175/JCLI-D-13-00740.1.

Pelly, J. L., and B. J. Hoskins, 2003: A new perspective on blocking. *J. Atmos. Sci.*, **60**, 743–755, doi:10.1175/1520-0469(2003)060<0743:ANPOB>2.0.CO;2.

Pfahl, S., and H. Wernli, 2012: Quantifying the relevance of atmospheric blocking for co-located temperature extremes in the Northern Hemisphere on (sub-)daily time scales. *Geophys. Res. Lett.*, **39**, L12807, doi:10.1029/2012GL052261.

Pook, M. J., J. S. Risbey, P. C. McIntosh, C. C. Ummenhofer, A. G. Marshall, and G. A. Meyers, 2013: The seasonal cycle of blocking and associated physical mechanisms in the Australian region and relationship with rainfall. *Mon. Wea. Rev.*, **141**, 4534–4553, doi:10.1175/MWR-D-13-00040.1.

Reeder, M. J., T. Spengler, and R. Musgrave, 2015: Rossby waves, extreme fronts, and wildfires in southeastern Australia. *Geophys. Res. Lett.*, **42**, 2015–2023, doi:10.1002/2015GL063125.

Reynolds, R. W., T. M. Smith, C. Liu, D. B. Chelton, K. S. Casey, and M. G. Schlax, 2007: Daily high-resolution-blended

analyses for sea surface temperature. *J. Climate*, **20**, 5473–5496, doi:10.1175/2007JCLI1824.1.

Sardeshmukh, P. D., and B. J. Hoskins, 1988: The generation of global rotational flow by steady idealized tropical divergence. *J. Atmos. Sci.*, **45**, 1228–1251, doi:10.1175/1520-0469(1988)045<1228:TGOGRF>2.0.CO;2.

Scherrer, S. C., M. Croci-Maspoli, C. Schwierz, and C. Appenzeller, 2006: Two-dimensional indices of atmospheric blocking and their statistical relationship with winter climate patterns in the Euro-Atlantic region. *Int. J. Climatol.*, **26**, 233–249, doi:10.1002/joc.1250.

Seth, A., K. Fernandes, and S. J. Camargo, 2015: Two summers of São Paulo drought: Origins in the western tropical Pacific. *Geophys. Res. Lett.*, **42**, 10 816–10 823, doi:10.1002/2015GL066314.

Sillmann, J., M. Croci-Maspoli, M. Kallache, and R. W. Katz, 2011: Extreme cold winter temperatures in Europe under the influence of North Atlantic atmospheric blocking. *J. Climate*, **24**, 5899–5913, doi:10.1175/2011JCLI4075.1.

Stefanon, M., F. D'Andrea, and P. Drobinski, 2012: Heatwave classification over Europe and the Mediterranean region. *Environ. Res. Lett.*, **7**, 014023, doi:10.1088/1748-9326/7/1/014023.

Thorncroft, C. D., B. J. Hoskins, and M. E. McIntyre, 1993: Two paradigms of baroclinic-wave life-cycle behaviour. *Quart. J. Roy. Meteor. Soc.*, **119**, 17–55, doi:10.1002/qj.49711950903.

Tibaldi, S., E. Tosi, A. Navarra, and L. Pedulli, 1994: Northern and Southern Hemisphere seasonal variability of blocking frequency and predictability. *Mon. Wea. Rev.*, **122**, 1971–2003, doi:10.1175/1520-0493(1994)122<1971:NASHSV>2.0.CO;2.

Trenberth, K. E., and K. C. Mo, 1985: Blocking in the Southern Hemisphere. *Mon. Wea. Rev.*, **113**, 3–21, doi:10.1175/1520-0493(1985)113<0003:BITSH>2.0.CO;2.

van der Wiel, K., A. J. Matthews, D. P. Stevens, and M. M. Joshi, 2015: A dynamical framework for the origin of the diagonal South Pacific and South Atlantic convergence zones. *Quart. J. Roy. Meteor. Soc.*, **141**, 1997–2010, doi:10.1002/qj.2508.

Vera C., and Coauthors, 2006: Toward a unified view of the American monsoon systems. *J. Climate*, **19**, 4977–5000, doi:10.1175/JCLI3896.1.

Webster, P. J., and H. R. Chang, 1998: Atmospheric wave propagation in heterogeneous flow: Basic flow controls on tropical–extratropical interaction and equatorial wave modification. *Dyn. Atmos. Oceans*, **27**, 91–134, doi:10.1016/S0377-0265(97)00003-1.

Widlansky, M. J., P. J. Webster, and C. D. Hoyos, 2011: On the location and orientation of the South Pacific convergence zone. *Climate Dyn.*, **36**, 561–578, doi:10.1007/s00382-010-0871-6.

Woollings, T., C. Czuchnicki, and C. Franzke, 2014: Twentieth century North Atlantic jet variability. *Quart. J. Roy. Meteor. Soc.*, **140**, 783–791, doi:10.1002/qj.2197.

Wright, W. J., 1994: Seasonal climate summary Southern Hemisphere (autumn 1993): A second mature ENSO phase. *Aust. Meteor. Mag.*, **43**, 205–212.

Zhang, C., 2005: Madden–Julian oscillation. *Rev. Geophys.*, **43**, RG2003, doi:10.1029/2004RG000158.